Fabrications and characterizations of high performance 1.2 kV, 3.3 kV, and 5.0 kV class 4H–SiC power SBDs*

Qing-Wen Song(宋庆文)[1,2,†], Xiao-Yan Tang(汤晓燕)[2,‡], Hao Yuan(袁昊)[2], Yue-Hu Wang(王悦湖)[2], Yi-Meng Zhang(张艺蒙)[2], Hui Guo(郭辉)[2], Ren-Xu Jia(贾仁需)[2], Hong-Liang Lv(吕红亮)[2], Yi-Men Zhang(张义门)[2], and Yu-Ming Zhang(张玉明)[2]

[1] *School of Advanced Materials and Nanotechnology, Xidian University, Xi'an* 710071, *China*
[2] *Key Laboratory of Wide Band Gap Semiconductor Materials and Devices, Xidian University, Xi'an* 710071, *China*

(Received 16 November 2015; revised manuscript received 7 January 2016; published online 20 February 2016)

In this paper, 1.2 kV, 3.3 kV, and 5.0 kV class 4H–SiC power Schottky barrier diodes（SBDs）are fabricated with three N-type drift layer thickness values of 10 μm, 30 μm, and 50 μm, respectively. The avalanche breakdown capabilities, static and transient characteristics of the fabricated devices are measured in detail and compared with the theoretical predictions. It is found that the experimental results match well with the theoretical calculation results and are very close to the 4H–SiC theoretical limit line. The best achieved breakdown voltages (BVs) of the diodes on the 10 μm, 30 μm, and 50 μm epilayers are 1400 V, 3320 V, and 5200 V, respectively. Differential specific-on resistances (R_{on-sp}) are 2.1 mΩ·cm^2, 7.34 mΩ·cm^2, and 30.3 mΩ·cm^2, respectively.

Keywords: 4H–SiC, Schottky-barrier diodes, breakdown，differential specific-on resistance

PACS: 71.20.Nr, 73.40.Sx, 77.22.Jp **DOI:** 10.1088/1674-1056/25/4/047102

1. Introduction

Silicon carbide (SiC) is one of the most promising wide band gap semiconductors for high power, high frequency, and high temperature electronic applications.[1–7] In particular, it can lead to a drastic reduction in size and weight of the power electronic system. The commercial availability of 4-inch (1 inch = 2.54 cm) wafer of 4H–SiC and the continuing efforts in scaling up SiC substrates by a number of companies are creating the basis for an emerging SiC power electronic industry.[8–15] The 4H–SiC Schottky barrier diode (SBD) as one of the major unipolar devices, is expected to replace the Si bipolar rectifier in a range from 600 V to 6500 V in the future due to its fast switching speed and low switching power dissipation. One of the typical applications of SiC SBDs is to serve as a fast diode employed in a power-factor-correction circuit of switching mode power supply.[16–19] Because of the negligibly small reverse recovery time of SiC Schottky barrier diode, the switching loss can be dramatically reduced and the switching frequency can be increased, leading to the downsizing of passive components. Since the first 1-kV SiC Schottky barrier diode with a low specific on resistance was demonstrated in 1993,[20,21] sustained efforts have been made to develop the SiC power Schottky barrier diode device technology and many 4H–SiC high voltage Schottky barrier diode devices have been demonstrated.[7–12,16,19,22] In the present paper, we report our newly developed high performance 1.2 kV, 3.3 kV, and 5.0 kV class 4H–SiC The first epitaxial layer sample (No .1) has a thickness of Schottky barrier diodes. 10 μm and a doping amount of 6.7 $\times 10^{15}\cdot$cm^{-3}. The second epitaxial layer sample (No. 2) has a thickness of 30 μm and a doping amount of 2.1 $\times 10^{15}\cdot$cm^{-3}. The third epitaxial layer sample (No. 3) has a thickness of 50 μm and a doping amount of 1.1 $\times 10^{15}\cdot$cm^{-3}. The Ti (for No. 1 and No. 2) and Ni (for No. 3) are employed as the Schottky contact metal.

2. Device design and Fabrication

2.1. Device structure and fabrication process

Figure 1(a) shows a simplified cross-sectional view of a 4H–SiC Schottky barrier diode fabricated and simulated in this paper. The 4H–SiC substrate is purchased from SICC Inc. Table 1 summarizes the values of epitaxial thickness (t_{epi}) and doping concentration (N_D) determined from the high frequency capacitance–voltage (HF C–V) characteristics of the different epitaxial layers used in this paper. In the table, the values of ideal breakdown voltage (IBV) of the three epitaxial layers with different thickness values, which are calculated using impact ionization coefficients, are also included. Figure 1(b) shows a major fabrication process flow of the 4H–SiC Schottky barrier diodes.

*Project supported by the National Natural Science Foundation of China (Grant Nos. 61404098, 61176070, and 61274079), the Doctoral Fund of Ministry of Education of China (Grant Nos. 20110203110010 and 20130203120017), the National Key Basic Research Program of China (Grant No. 2015CB759600), and the Key Specific Projects of Ministry of Education of China (Grant No. 625010101).

†Corresponding author. E-mail: qwsong@xidian.edu.cn
‡Corresponding author. E-mail: xytang@mail.xidian.edu.cn

© 2016 Chinese Physical Society and IOP Publishing Ltd

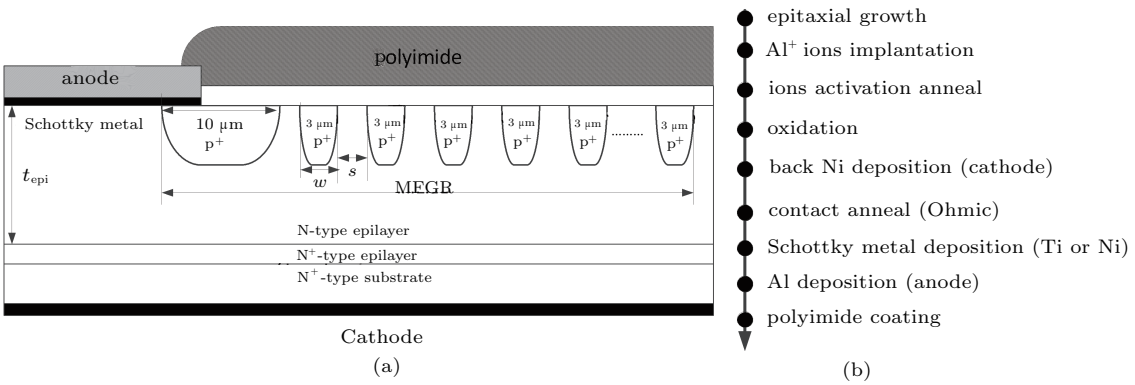


Fig. 1. Simplified cross-sections of the fabricated and simulated 4H–SiC SBD structure (a) and fabrication process flow (b).

The fabrication process starts from a standard cleaning process, after which the native oxide was stripped in dilute hydrofluoric (HF) acid. Next, aluminum (Al) was ion implanted to form the multiple floating guard rings (MFGR) termination. The Al implanted epitaxial layers were annealed at 1700 °C for 30 min to electrically activate Al ions. A graphite film was used to suppress degradation in the electrical properties of SBDs by activation annealing. The graphite film was removed by oxidation at 1100 °C for 1 h after the activation annealing, followed by surface passivation with plasma enhanced chemical vapor deposition (PECVD) oxide. Then, Ni was sputtered on the back cathode region. The Ohmic contact annealing was carried out at 1000 °C for 5 min by using a rapid thermal processing (RTP) system. Ti or Ni film was also deposited and patterned to form the front Schottky contact. After ohmic and Schottky contact formation, about 4-μm Al was sputtered to form a thick overlay metal on the anode and cathode separately to improve the voltage and current distribution. Finally, a thick polyimide was coated as the last passivation layer. The active area size of fabricated devices were all 4 mm^2.

Table 1. Thickness values and doping concentrations of 4H-SiC epilayer employed for SBD fabrication.

Epi	t_{epi}/μm	N_D/cm^{-3}	IBV/V
		Extracted from *C*–*V* measurements	
No. 1	10	6.7×10^{15}	1762 (∼ 1.2-kV class)
No. 2	30	2.1×10^{15}	4627 (∼ 3.3-kV class)
No. 3	50	1.1×10^{15}	7482 (∼ 5.0-kV class)

2.2. Junction termination design

To achieve a nearly ideal breakdown voltage of the fabr cated 4H–SiC SBD, the MFGR junction termination structu was adopted, designed and optimized with an ISE-DESSI simulator. To achieve the nearly ideal breakdown voltage, th key is to optimize the MFGR width (w) and space (s). The ob jective of the MFGR is to reduce the electric field at the edg of Schottky contact and make the electric field distributio more uniform through the termination region. The obtaine optimum designs for the 4H–SiC SBDs have 57 μm-wid MFGR with 10 rings (epitaxial thickness: 10 μm), 176 μn wide MFGR with 32 rings (epitaxial thickness: 30 μm and 375 μm-wide MFGR with 65 rings (epitaxial thickne 50 μm), respectively. Figure 2 shows electric field distribu tions of the 4H–SiC SBDs with optimum MFGR termination at the breakdown point. The simulated breakdown voltages of the optimized MFGR were 1460 V for the 10-μm epilayer, 3890 V for the 30-μm epilayer, and 6100 V for the 50-μm epilayer, respectively. The breakdown voltage was achieved when the integral ionization was equal to one.

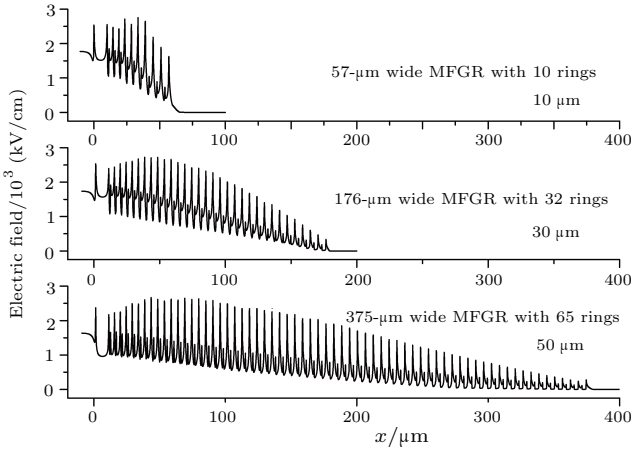


Fig. 2. Simulated electric field distributions of the 4H-SiC SBDs with optimum MFGR termination at breakdown point.

3. Experimental results and discussion

3.1. Forward characteristics

Figure 3 shows the forward current density–voltage (J_F–V) characteristics of SiC SBDs fabricated with wafers No. 1–No. 3. The Schottky contact metals are Ti for the 1.2-kV and

3.3-kV class diode and Ni for the 5.0-kV class diode, respectively. Therefore, the turn-on voltages are 0.9 V for the 1.2-kV and 3.3-kV diodes and 1.2 V for the 5.0-kV class diodes, respectively. The Schottky barrier heights (SBHs) are estimated to be 1.2 eV and 1.6 eV for Ti/4H–SiC and Ni/4H–SiC, respectively, as derived from the low-current log–linear portion of the *I*–*V* curves (not shown). The values of forward voltage (V_F) of the 1.2-kV, 3.3-kV, and 5.0-kV class SBDs are 1.15 V, 1.66 V, and 3.97 V respectively, when the forward current density (J_F) is 100 A/cm^2 at room temperature. The differential values of on-resistance (R_{on-sp}) at a current density of 100 A/cm^2 are measured to be 30.3 m$\Omega\cdot$cm^2, 7.34 m$\Omega\cdot$cm^2, and 2.1 m$\Omega\cdot$cm^2 for the 5.0-kV, 3.3-kV, and 1.2-kV classes respectively. As epitaxial thickness increases, the differential on-resistance significantly increases.

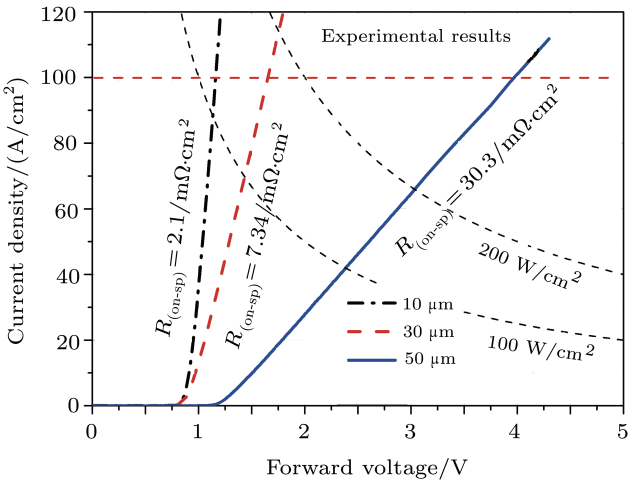


Fig. 3. (color online) Forward current density–voltage characteristics of SiC SBDs fabricated with wafers No. 1–No. 3 having different epitaxial thickness values (10 μm, 30 μm, and 50 μm).

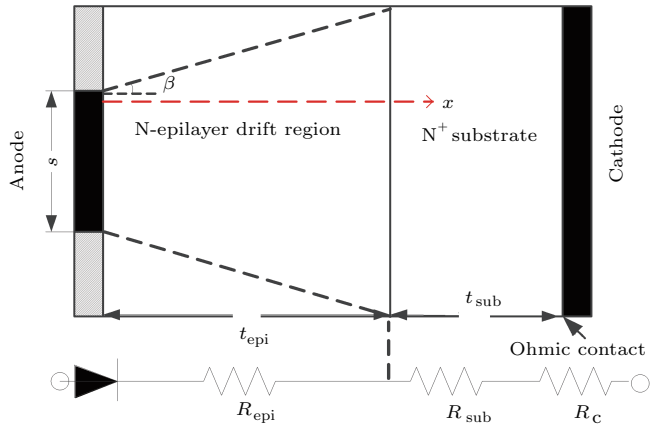


Fig. 4. (color online) Cross-sectional view of the model structure of SBD.

Owing to the current flow with the lateral effect in the epitaxial layer of power SBD device, the active area is larger than the anode area. Therefore, the forward conduction of 4H–SiC SBD can be a model as shown in Fig. 4 according to the current flow pattern in the SBD, where a parameter β is introduced to reflect the current lateral spreading effect. β values are 45° for 10-μm epilayer, 35° for 30-μm epilayer, and 30° for 50-μm epilayer, respectively, determined from the numerical simulations. Based on this model, the on-resistance can be divided into three different components: Ohmic contact resistance, epilayer spreading resistance, and substrate resistance. Thus the series resistance can be expressed as[23]

$$R_{on} = R_c + R_{epi} + R_{sub}, \tag{1}$$

where R_{epi} is the epitaxial layer resistance, R_c is the Ohmic contact resistance, and R_{sub} is the substrate resistance. For the ideal R_{on-sp}, the Ohmic contact resistance R_c is usually neglected due to the fact that its value is far smaller than those of epitaxial layer resistance and substrate resistance. Therefore, the ideal R_{on-sp} is shown as follows:

$$R_{on-sp} = R_{epi-sp} + R_{sub-sp}. \tag{2}$$

The epitaxial layer resistance is a trapezoid, which can be obtained by integration of dR_{epi} along the x direction (as shown in Fig. 4) between the surface ($x = 0$) and the N$^+$ substrate ($= t_{epi}$):[23]

$$\mathrm{d}R_{epi} = \rho_D \frac{\mathrm{d}x}{S + 2x\tan\beta}, \tag{3}$$

$$\begin{aligned} R_{epi-sp} &= (S + 2t_{epi}\tan\beta)\cdot R_{epi} \\ &= (S + 2t_{epi}\tan\beta)\cdot \int_0^{t_{epi}} \rho_D \frac{\mathrm{d}x}{S + 2x\tan\beta} \\ &= (S + 2t_{epi}\tan\beta)\left(\frac{1}{qN_{epi}\mu_n}\right)\int_0^{t_{epi}} \frac{\mathrm{d}x}{S + 2x\tan\beta} \\ &= (S + 2t_{epi}\tan\beta)\cdot\left(\frac{1}{qN_{epi}\mu_n}\right) \\ &\quad \times \frac{1}{2\tan\beta}\ln\left(\frac{S + 2t_{epi}\tan\beta}{S}\right). \end{aligned} \tag{4}$$

The substrate resistance can be calculated from

$$\begin{aligned} R_{sub,sp} &= (S + 2t_{epi}\tan\beta)\cdot R_{sub} = (S + 2t_{epi}\tan\beta) \\ &\quad \times \rho_D \frac{t_{sub}}{S + 2t_{epi}\tan\beta} = \left(\frac{1}{qN_{sub}\mu_n}\right)\cdot t_{sub}. \end{aligned} \tag{5}$$

Therefore, the ideal R_{on-sp} can be expressed as follows:

$$R_{on-sp} = \frac{S + 2t_{epi}\tan\beta}{qN_D\mu_n \cdot 2t_{epi}\tan\beta}\ln\left(\frac{S + 2t_{epi}\tan\beta}{S}\right) + \frac{t_{sub}}{qN_{sub}\mu_n}, \tag{6}$$

where N_D and N_{sub} are the doping concentrations of the epilayer and substrate, respectively, t_{epi} is the thickness of the epilayer, t_{sub} is the thickness of substrate, ρ_D is the resistivity of the 4H–SiC, μ_n is the electron mobility of 4H–SiC, and $S = 2$ mm is the Schottky junction width. Using this model, differential on-resistance can be calculated. The relationships between differential on-resistance and epilayer doping are plotted in Fig. 5 and compared with those obtained from experiments. It can be seen that the two sets of data show high consistency. Experimental results are very close to the ideal theoretical values of differential on-resistance determined by the epitaxial thickness and doping concentration.

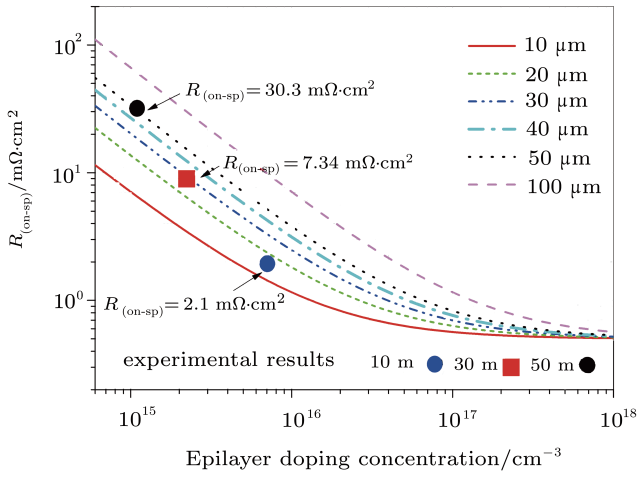


Fig. 5. (color online) Relationships between differential on-resistance and epilayer doping concentration.

3.2. Reverse Blocking characteristics

The reverse blocking characteristics of fabricated 4H–SiC SBDs based on epitaxial layers with different thickness values are in Fig. 6.

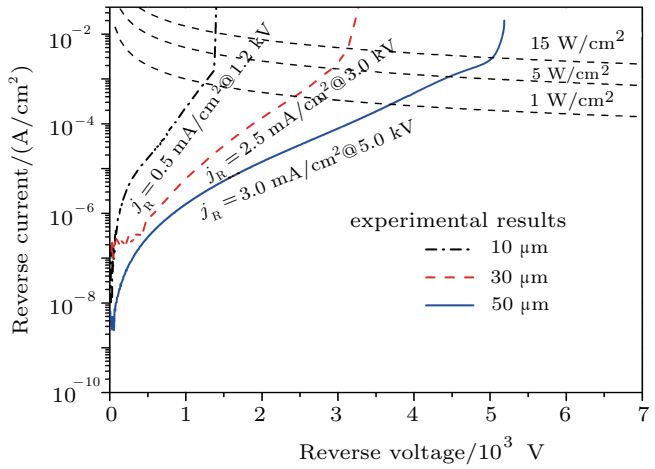


Fig. 6. (color online) Reverse leakage current density characteristics (J_R–V) of the fabricated 4H–SiC SBDs based on epitaxial layers with different thickness values.

The dc blocking characteristic test is done in a probe station that is capable of testing the case of up to 10 kV. It can be seen that a sharp avalanche behavior is observed at reverse voltages of 1.4 kV (epitaxial thickness: 10 μm), 3.32 kV (epitaxial thickness: 30 μm), and 5.2 kV (epitaxial thickness: 50 μm), respectively. Figure 6 also shows the reverse leakage current density characteristics (J_R–V) of diodes of the three types. The leakage current densities are 0.4 mA/cm^2 at 1.2 kV, 0.96 mA/cm^2 at 30 kV, and 0.96 mA/cm^2 at 5.0 kV, respectively. Below the avalanche breakdown point, the J_R rapidly increases with the reverse voltage increasing. The J_R–V curves of those devices are produced by the typical thermionic field emission mechanisms, which leads to a barrier lowering effect proportional to the square of the electric field at the Schottky metal/semiconductor interface. The cases for dissipation powers per unit at 1 W/cm^2, 5 W/cm^2, and 15 W/cm^2 for the fabricated three types of 4H–SiC SBDs are also presented in Fig. 6. In the case of the 5-kV 4H–SiC Schottky diode, the reverse power dissipation at room temperature is slightly less than 15 W/cm^2, and for 1.2-kV and 3.3 kV-classes diodes, the reverse dissipation powers are 0.6 W/cm^2 and 7.5 W/cm^2 at reverse voltages of 1.2 kV and 3.0 kV, respectively.

3.3. Reverse recovery characteristics

The reverse recovery transients of the 1.2-kV, 3.0-kV, and 5.0-kV 4H–SiC SBDs at room temperature are shown in Fig. 7. Under the test conditions adopted, the devices are switched from the forward current of 0.5 A to the blocking state with a reverse bias of 10 V at a current rate-of-fall of 25 A/μs. For 5.0-kV 4H–SiC SBD, the diode has a reverse recovery time t_{rr} of 17.35 ns, a peak reverse current $I_{RM(rec)}$ of 0.064 A, and a reverse recovery charge Q_{rr} of 1.402 nC. Table 2 summarizes the reverse recovery characteristics for the three types of SBDs. Since the reverse recovery current of a majority carrier diode (pure Schottky structure) is purely capacitive in nature, t_{rr}, $I_{RM(rec)}$, and Q_{rr} are only dependent on the epitaxial doping concentration. As the epitaxial doping concentration increases, the reverse recovery transient time increases.

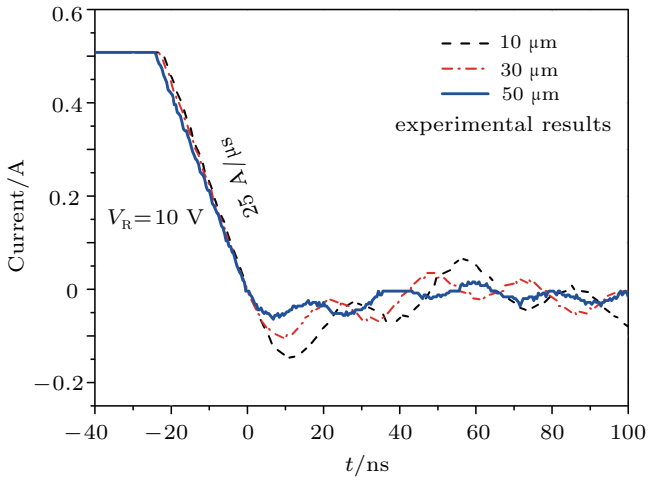


Fig. 7. (color online) Reverse recovery transient characteristics of the fabricated 4H-SiC SBDs at room temperature.

Table 2. Reverse recovery characteristics of the fabricated 4H–SiC SBDs at room temperature.

Type/kV	t_{rr}/ns	$I_{RM(rac)}$)/A	Q_{rr}/nC	Q_c/nC
1.2	27.59	0.168	3.460	3.612
3.3	22.47	0.108	2.452	2.522
5	17.35	0.064	1.402	1.516

Figure 8 shows the high frequency (1 MHz) capacitance–voltage (C–V) curves for 10-, 30-, and 50-μm 4H–SiC SBDs. The inset displays the inverse square of capacitance ($1/C^2$) as a function of gate voltage (V). The C–V data are measured over a gate voltage range from 0 V to −10 V. The epitaxial drift layer doping concentration N_D can be extracted by employing

a linear extrapolation of $1/C^2$ versus V. The extracted N_D values for the No. 1, No. 2, and No. 3 wafers are presented in Table 1. Form the C–V curves, the total junction capacitance charge Q_c can be extracted. For the three types of 4H–SiC SBDs measured, the average capacitive charge extrapolated to -10V is very close to the Q_{rr} calculated from the reverse recovery transient, confirming that the reverse recovery current is entirely capacitive in nature.

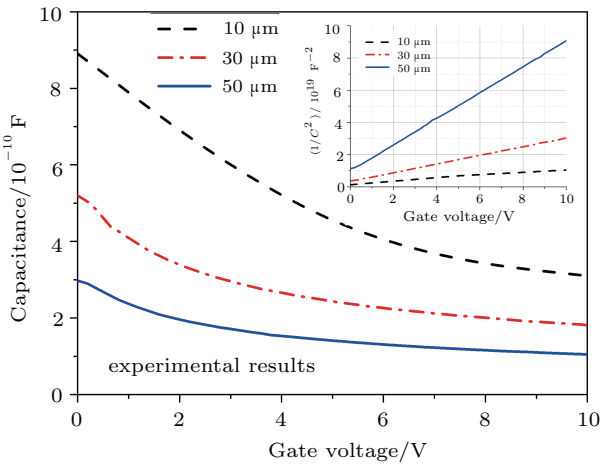


Fig. 8. (color online) High frequency (1 MHz) C–V curves for the fabricated 4H–SiC SBDs, with the inset showing the $1/C^2$ versus V.

3.4. Tradeoff between specific on-resistance and breakdown voltage

For the unipolar power device such as Schottky diode, there is a tradeoff between specific on-resistance and breakdown voltage. For a certain rated breakdown voltage (BV), the ideal on-resistance of the device depends on the dielectric constant, the carrier mobility, and the critical electric field of semiconductor material. The on-resistance can be expressed as follows:

$$R_{on-sp} = \frac{4V_B^2}{\varepsilon_s \mu_n E_C^3}, \tag{7}$$

where ε_s is the dielectric constant, μ_n is the electron mobility, E_C is the breakdown electric field, V_B is the breakdown voltage, $\varepsilon_s \mu_n E_C^3$ is called the Baliga figure of merit (BFOM), which is commonly used to qualitatively evaluate the device characteristics. Figure 9 shows the curves of tradeoff between the specific on-resistance and the breakdown voltage. Solid diagonal lines in the figure represent the theoretical limits for silicon and 4H–SiC with the contribution of the substrate. The performances of a number of reported SiC power SBDs are also presented. The device fabricated in our group is also included for comparison. It can be seen that the performances of our present 4H–SiC SBDs are very close to the 4H–SiC theoretical limit. Moreover, the V_B^2/R_{on-sp} values of our reported 4H–SiC SBDs are calculated to be 933 MW/cm^2, 1501 MW/cm^2, and 892 MW/cm^2, respectively. The best V_B^2/R_{on-sp} value is obtained in the 3.32 kV device.

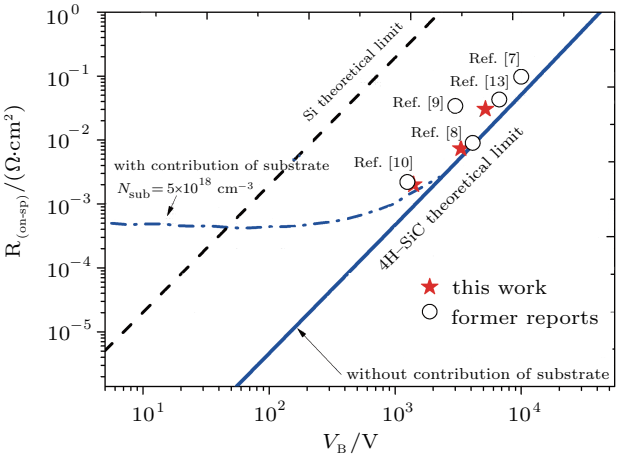


Fig. 9. (color online) Plots of specific on-resistance versus breakdown voltage for Schottky barrier diodes (380-μm thick 5×10^{18} cm^{-3} nitrogen doped substrate) with and without contribution of substrate.

4. Conclusions

High-performance 4H–SiC power SBDs with three N-type drift layer thickness values of 10 μm, 30 μm, and 50 μm are designed and fabricated in this paper. The presented devices show excellent avalanche breakdown capabilities, static characteristics, and reverse recovery transients. The performances of the fabricated devices are very close to the 4H–SiC theoretical limit line. We successfully obtain a 4H–SiC SBD fabricated on a 30-μm thick 2.1×10^{15} cm^{-3} nitrogen-doped epilayer with a breakdown voltage of 3.32 kV and a differential specific-on resistance (R_{on-sp}) of 7.34 mΩ·cm^2, achieving a best V_B^2/R_{on-sp} value of 1501 MW/cm^2. We also obtain 4H–SiC SBDs, each of which is fabricated on a 50-μm thick 1.1×10^{15} cm^{-3} nitrogen-doped epilayer and has a breakdown voltage of 5.2 kV and an on-line resistance R_{on-sp} of 30.1 mΩ·cm^2.

References

[1] Kaji N, Niwa H, Suda J and Kimoto T 2015 *IEEE Trans. Electron Dev.* **62** 373
[2] Sung W, Van Brunt E, Baliga B J and Huang A Q 2011 *IEEE Electron Dev. Lett.* **32** 880
[3] Song Q W, Yuan H, Han C, Zhang Y M, Tang X Y, Zhang Y M, Guo H, Zhang Y M, Jia R X and Wang Y H 2015 *Sci. China-Tech. Sci.* **58** 1369
[4] Song Q W, Zhang Y M, Zhang Y M and Tang X Y 2012 *Diamond Relat. Mater.* **22** 42
[5] Wang Y, Yu C, Miao Z and Shan M G 2015 *IET Power Electron.* **8** 672
[6] Yuan H, Tang X Y, Zhang Y M, Zhang Y M, Song Q W, Yang F and Wu H 2014 *Chin. Phys. B* **23** 057102
[7] Zhao J H, Alexandrov P and Li X 2003 *IEEE Electron Dev. Lett.* **24** 402
[8] Nakamura T, Miyanagi T, Kamata I, Jikimoto T and Tsuchida H 2005 *IEEE Electron Dev. Lett.* **26** 99
[9] Wahab Q, Kimoto T, Ellison A, Hallin C, Tuominen M, Yakimova R, Henry A, Bergman J P and Janzen E 1998 *Appl. Phys. Lett.* **72** 26

[10] Morisette D T, Cooper J A, Melloch M R, Dolny G M, Shenoy P M, Zafrani M and Gladish J 2001 *IEEE Trans. Electron Dev.* **48** 349
[11] Huang R H, Chen G, Bai S, Li R, Li Y and Tao Y H 2014 *Mater. Sci. Forum.* **778–780** 800
[12] Vassilevski K, Nikitina I, Horsfall A, Wright N G, O'Neill A G, Hilton K P, Munday A G, Hydes A J, Uren M J and Johnson C M 2007 *Mater. Sci. Forum.* **556–557** 873
[13] Song Q W, Zhang Y M, Zhang Y M, Zhang Q and Lu H L 2010 *Chin. Phys. B* **19** 087202
[14] Song Q W, Zhang Y M, Han J S, Tanner P, Dimitrijev S, Zhang Y M, Zhang Y M, Tang X Y and Guo H 2013 *Chin. Phys. B* **22** 027302
[15] Trentin A, Zanchetta P, Wheeler P and Clare J 2012 *IET Power Electron.* **5** 1873
[16] Ying W, Likun X and Kun D 2014 *IET Power Electron.* **7** 325
[17] Zhao J H, Li X, Tone K, Alexandrov P, Pan M and Weiner M 2003 *Solid-State Electron.* **47** 377
[18] Kimoto T 2015 *Jpn. J. Appl. Phys.* **54** 040103
[19] Kimoto T, Urushidani T, Kobayashi S and Matsunami Hiroyuki 1993 *IEEE Electron Dev. Lett.* **14** 548
[20] Wadaa K, Uchida K, Kimura R, Sakai M, Hatsukawa S, Hiratsuka K, Hirakata N and Mikamura Y 2014 *Mater. Sci. Forum.* **778–780** 915
[21] Bartolf H, Sundaramoorthy V, Mihaila A, Berthou M, Godignon P and Millán J 2014 *Mater. Sci. Forum.* **778** 795
[22] Song Q W, Zhang Y M, Zhang Y M, Chen F P and Tang X Y 2011 *Chin. Phys. B* **20** 057301
[23] Baliga B J 2009 *Advanced power rectifier concepts* (New York: Springer Science + Business Media, LLC) pp. 45–48